

# Geophysical Research Letters®

## RESEARCH LETTER

10.1029/2021GL097133

### Key Points:

- The global surface temperature responds asymmetrically to increased and decreased CO<sub>2</sub> levels, in both abrupt and transient cases
- Effective climate sensitivity is higher with warming (2×, 4×, 8×CO<sub>2</sub>) than with cooling (1/2×, 1/4×, 1/8×CO<sub>2</sub>), in two different coupled models
- The non-logarithmic nature of the CO<sub>2</sub> forcing is primarily responsible for the asymmetry, not the radiative feedbacks

### Supporting Information:

Supporting Information may be found in the online version of this article.

### Correspondence to:

I. Mitevski,  
im2527@columbia.edu

### Citation:

Mitevski, I., Polvani, L. M., & Orbe, C. (2022). Asymmetric warming/cooling response to CO<sub>2</sub> increase/decrease mainly due to non-logarithmic forcing, not feedbacks. *Geophysical Research Letters*, 49, e2021GL097133. <https://doi.org/10.1029/2021GL097133>

Received 24 NOV 2021

Accepted 25 FEB 2022

## Asymmetric Warming/Cooling Response to CO<sub>2</sub> Increase/Decrease Mainly Due To Non-Logarithmic Forcing, Not Feedbacks

Ivan Mitevski<sup>1</sup>, Lorenzo M. Polvani<sup>1,2</sup>, and Clara Orbe<sup>1,3</sup>

<sup>1</sup>Department of Applied Physics and Applied Mathematics, Columbia University, New York, NY, USA, <sup>2</sup>Lamont-Doherty Earth Observatory, Columbia University, Palisades, NY, USA, <sup>3</sup>NASA Goddard Institute for Space Studies, New York, NY, USA

**Abstract** We explore the CO<sub>2</sub> dependence of effective climate sensitivity ( $S_G$ ) with symmetric abrupt and transient CO<sub>2</sub> forcing, spanning the range 1/8×, 1/4×, 1/2×, 2×, 4×, and 8×CO<sub>2</sub>, using two state-of-the-art fully coupled atmosphere-ocean-sea-ice-land models. In both models, under abrupt CO<sub>2</sub> forcing, we find an asymmetric response in surface temperature and  $S_G$ . The surface global warming at 8×CO<sub>2</sub> is more than one third larger than the corresponding cooling at 1/8×CO<sub>2</sub>, and  $S_G$  is CO<sub>2</sub> dependent, increasing non-monotonically from 1/8×CO<sub>2</sub> to 8×CO<sub>2</sub>. We find similar CO<sub>2</sub> dependence in the transient runs, forced with  $-1\text{yr}^{-1}\text{CO}_2$  and  $+1\text{yr}^{-1}\text{CO}_2$  up to 1/8×CO<sub>2</sub> and 8×CO<sub>2</sub>, respectively. The non-logarithmic radiative forcing—not the changing feedbacks—primarily explains the dependence of  $S_G$  on CO<sub>2</sub>, particularly at low CO<sub>2</sub> levels. The changing feedbacks, however, explain  $S_G$ 's non-monotonic behavior.

**Plain Language Summary** Equilibrium climate sensitivity is the global mean warming after doubling CO<sub>2</sub> concentrations from those of the year 1850. Since CO<sub>2</sub> levels will likely surpass a doubling, it is crucial to know whether the amount of warming per CO<sub>2</sub> doubling (which we refer to as the effective climate sensitivity,  $S_G$ ) is constant with each CO<sub>2</sub> doubling or whether it changes. Necessary conditions for constant  $S_G$  are (a) the radiative forcing introduced to the climate system from each CO<sub>2</sub> doubling is constant and (b) the net radiative feedback does not change with CO<sub>2</sub> levels. Current literature shows that  $S_G$  will increase in a warmer world because the radiative feedback will change. We here investigate  $S_G$  in both warmer and colder worlds, and confirm that  $S_G$  increases at higher CO<sub>2</sub> concentrations. However, we show that changes in the radiative forcing with each CO<sub>2</sub> doubling are mainly responsible for  $S_G$  increase with CO<sub>2</sub>, not feedback changes.

## 1. Introduction

Equilibrium climate sensitivity (ECS) is the global mean surface temperature change after the doubling of CO<sub>2</sub> concentrations from pre-industrial (PI) levels. ECS is perhaps the most important metric in climate science, and it has been extensively investigated in the literature (Sherwood et al., 2020). An important question is whether the amount of warming for each CO<sub>2</sub> doubling (which we refer to as the effective climate sensitivity,  $S_G$ ) is constant or not (i.e., whether it is CO<sub>2</sub> dependent). Necessary conditions for a constant  $S_G$  are (a) that the radiative forcing of the climate system for each CO<sub>2</sub> doubling is constant and (b) that the net radiative feedback does not change with CO<sub>2</sub> levels. This question has been investigated in many modeling studies (Bloch-Johnson et al., 2021; Meraner et al., 2013; Mauritsen et al., 2019; Sherwood et al., 2020), which have reported that  $S_G$  is indeed CO<sub>2</sub> dependent. Most of these studies find that  $S_G$  increases at higher CO<sub>2</sub> levels and that the change in feedbacks, not the change in CO<sub>2</sub> radiative forcing, is the primary driver of  $S_G$  CO<sub>2</sub> dependence.

An alternative approach to using climate models to investigate the dependency of  $S_G$  on CO<sub>2</sub> is to seek observational constraints from reconstructions of past climates. In particular, most studies conclude that  $S_G$  inferred from paleoclimate records does depend on CO<sub>2</sub> (Anagnostou et al., 2016, 2020; Caballero & Huber, 2013; Farnsworth et al., 2019; Friedrich et al., 2016; Shaffer et al., 2016; Zhu et al., 2019), although a few studies disagree (e.g., Martínez-Botí et al., 2015). An ideal period to study the  $S_G$  from past climate is the Last Glacial Maximum (LGM), approximately 21 kyr ago, when the Earth was roughly 6K colder than PI conditions (Tierney et al., 2020). The LGM period is of particular interest because the climate system was in a quasi-equilibrium state, the climate forcings were large, and the surface temperature reconstructions are relatively well-constrained (Zhu & Poulsen, 2021). However, when considering the LGM and other periods in Earth's past, one needs to account

for how the feedbacks in those past climate states differ from the feedbacks operating in the modern state: hence the challenge in using paleoclimate-based estimates to constrain  $S_G$ .

While modeling and paleoclimatic evidence suggest that  $S_G$  depends on  $\text{CO}_2$ , a systematic exploration of the symmetry over a wide range of  $\text{CO}_2$  forcing has yet to be performed. The question thus remains: is the climate system response symmetric across a broad range of positive (warm) and negative (cold)  $\text{CO}_2$  forcings? The question of symmetry was examined recently by Chalmers et al. (2022), who compared  $1/2\times$  and  $2\times\text{CO}_2$  simulations performed with the CESM1-CAM5 model, and found that global surface temperatures warm 20% more than they cool. Roughly 50% of this asymmetry was shown to derive from an asymmetry in  $\text{CO}_2$  radiative forcing; the rest was associated with differences in feedbacks which, interestingly, were found not to be related to clouds. Whether this result holds over a broader range of  $\text{CO}_2$  forcing, and whether it is model dependent remains an open question.

We here address these questions using a much broader range of both abrupt and transient  $\text{CO}_2$  forcings, and do so with two different climate models. Specifically,  $\text{CO}_2$  is varied from  $1/8\times$  to  $8\times\text{PI}$  values, to test the  $\text{CO}_2$  symmetry of the climate system response to comparable increased and decreased  $\text{CO}_2$ . While we are not the first ones to perform such symmetric  $\text{CO}_2$  runs (Chalmers et al., 2022; Colman & McAvaney, 2009; Hansen et al., 2005; Russell et al., 2013), here we explore (a) a larger  $\text{CO}_2$  range than previously considered, (b) we do so using two different fully coupled climate models and, most importantly, (c) we perform the experiments with both abrupt and transient  $\text{CO}_2$  runs.

Overall we confirm the asymmetric response in surface temperature: the climate system warms *more* with consecutive  $\text{CO}_2$  doublings ( $2\times$ ,  $4\times$ , and  $8\times\text{CO}_2$ ) than it cools with consecutive  $\text{CO}_2$  halvings ( $1/2\times$ ,  $1/4\times$ , and  $1/8\times\text{CO}_2$ ). This asymmetry is also reflected in  $S_G$ , which *increases* at higher  $\text{CO}_2$  concentrations, consistent with previous studies. Surprisingly, we find that the non-logarithmic dependence of  $\text{CO}_2$  radiative forcing (i.e., the fact that  $\text{CO}_2$  radiative forcing increases more rapidly than the log of the  $\text{CO}_2$  concentration) is primarily responsible for this asymmetric response, and not the changes in radiative feedbacks.

## 2. Methods

### 2.1. Models Used

We use two fully coupled atmosphere-ocean-sea-ice-land models: the large ensemble version of the Community Earth System Model (CESM-LE) and the NASA Goddard Institute for Space Studies Model E2.1-G (GISS-E2.1-G). CESM-LE comprises the Community Atmosphere Model version 5 (CAM5, 30 vertical levels), and parallel ocean program version 2 (POP2, 60 vertical levels) with approximately  $1^\circ$  horizontal resolution in all model components (Kay et al., 2015). GISS-E2.1-G is a 40-level atmospheric model with a resolution of  $2^\circ \times 2.5^\circ$  latitude/longitude, coupled to a  $1^\circ$  horizontal resolution 40-level GISS Ocean v1 (GO1) (Kelley et al., 2020). This configuration of the GISS model contributed to the CMIP6 project under the label “GISS-E2.1-G.” We show CESM-LE results in the main text, and some GISS-E2.1-G results in supplementary information (SI) to corroborate CESM-LE findings.

### 2.2. Abrupt $n\times\text{CO}_2$ Experiments

We perform a series of abrupt  $\text{CO}_2$  forcing runs using both models, subject to  $1/8\times$ ,  $1/4\times$ ,  $1/2\times$ ,  $2\times$ ,  $4\times$ , and  $8\times\text{CO}_2$  forcings, with all other trace gases, ozone concentrations, aerosols, and other forcings fixed at PI values. Following CMIP6 protocol for  $4\times\text{CO}_2$  runs, we integrate all runs to 150 years starting from PI conditions. We contrast these to a PI control run to calculate the response.

For each model, we estimate the effective radiative forcing (ERF) with a companion series of  $\text{CO}_2$  experiments, as per Forster et al. (2016), with prescribed PI sea surface temperatures (SSTs) and sea-ice concentrations (SICs). These experiments are 30-year-long. We calculate ERF as the difference between the global mean net top of the atmosphere (TOA) flux between PI and  $n\times\text{CO}_2$  in these prescribed SSTs and SICs experiments. We do not here adjust for land warming simply because, in our ERF calculations, the surface temperature response in the fixed SSTs and SICs simulations is minimal (Smith et al., 2020), but we have verified that the adjustment does not change our results (see Figure S3 in Supporting Information S1).

### 2.3. Transient Experiments

In addition to the abrupt CO<sub>2</sub> runs, we also perform transient CO<sub>2</sub> runs with the CESM-LE model. We start from PI conditions (same as in the abrupt CO<sub>2</sub> forcing), and we increase CO<sub>2</sub> at +1%yr<sup>-1</sup> for the “warm” case for 215 years (slightly above 8×CO<sub>2</sub>) and −1%yr<sup>-1</sup> for the “cold” case for 215 years (slightly below 1/8×CO<sub>2</sub>). We estimate transient ERF as in the abrupt experiments, by running companion simulations with specified SSTs and SICs set to PI values (Forster et al., 2016), while ramping up CO<sub>2</sub> at rates of +1%yr<sup>-1</sup> and −1%yr<sup>-1</sup>. We contrast all variables to PI values to compute the response.

### 2.4. Climate Sensitivity and Feedbacks

We define effective climate sensitivity  $S_G$  as the  $x$ -intercept of the Gregory regression (Gregory et al., 2004) for each abrupt  $n \times \text{CO}_2$  run using the following equation:

$$S_G = \left| \frac{F_{y-\text{int}}(n \times \text{CO}_2)}{\lambda(n \times \text{CO}_2) \cdot \log_2 n} \right| \quad (1)$$

We find the radiative forcing  $F_{y-\text{int}}$  as the  $y$ -intercept and the net feedback parameter  $\lambda$  as the slope from the Gregory regression (see Figure S1 in Supporting Information S1) where we regress the net TOA radiative imbalance against the global mean surface temperature response for years 1–150. In order to compare  $S_G$  for different CO<sub>2</sub> doubling/halving, we divide by  $\log_2 n$  (assuming a logarithmic CO<sub>2</sub> forcing) and take the absolute value in Equation 1. Note that our definition of the effective climate sensitivity  $S_G$  is a generalization of the more common definition of effective climate sensitivity (which is typically defined as per Equation 1 but with  $n = 2$ ). To check for the possibility that  $\lambda$  and  $S_G$  may be strongly affected by the “pattern effect”, we have repeated the calculations by regressing years 21–150 only, and our main results were not changed.

To calculate the individual feedbacks  $\lambda_x$ , we use radiative kernels ( $K_x$ ) from both Huang et al. (2017) and Pendergrass et al. (2018) to quantify the sensitivity of TOA radiation imbalance ( $\Delta R$ ) to changes in surface and atmospheric temperature ( $T$ ), water vapor ( $q$ ), and surface albedo ( $\alpha$ ) (Shell et al., 2008; Soden et al., 2008). For each year of the 150-year experiment, we multiply the spatially resolved kernels by the climate field anomalies ( $R_x = K_x \cdot \Delta x$ , where  $x$  is  $T$ ,  $q$ ,  $\alpha$ ), and then vertically integrate (for atmospheric temperature and water vapor) up to the tropopause. We define the tropopause as 100 hPa at the equator, 300 hPa at the poles, and in between, it varies by the cosine of the latitude (Soden & Held, 2006). Lastly, we regress these quantities on the surface temperature response to find the radiative feedbacks as the regression slope. The cloud feedbacks are computed via the residual method (Soden & Held, 2006) as follows. First, we subtract ERF and the temperature, water vapor, and surface albedo radiative fluxes from the TOA net radiative flux, resulting in  $\Delta R_{\text{cloud}} = \Delta R - \text{ERF} - \sum \Delta R_x$ . Then, we regress  $\Delta R_{\text{cloud}}$  onto  $\Delta T_s$  anomalies and define the corresponding slope as the cloud feedback. Lastly, we find shortwave (SW) and longwave (LW) components of the cloud feedback by considering the radiative changes in LW and SW components separately.

In the transient runs, we estimate the net feedback parameter  $\lambda_{\text{tr}}$  following Rugenstein and Armour (2021) (see  $\lambda_{\text{eff1pet}}$  in their Figure 1d) with the expression:

$$\lambda_{\text{tr}} = - \frac{\text{ERF}(t) - \Delta R(t)}{\Delta T_s(t)} \quad (2)$$

$\Delta R(t)$  is the net TOA radiative imbalance, and  $\Delta T_s(t)$  is the global mean surface temperature response in the transient runs at year  $t$ .  $\Delta R(t)$  and  $\Delta T_s(t)$  are 30-year moving averages of the respective terms. Note that we use different definitions for the feedback parameter in the abrupt and transient simulations.

## 3. Results

### 3.1. Abrupt CO<sub>2</sub> Experiments

We start by examining the global mean surface temperature response ( $|\Delta T_s|$ ) timeseries for the abrupt CO<sub>2</sub> runs (Figure 1). We contrast—in panels a, b, and c—the timeseries of each corresponding “warm” (2×, 4×, and 8×CO<sub>2</sub>) and “cold” simulation (1/2×, 1/4×, and 1/8×CO<sub>2</sub>) by taking the absolute value of the response from PI:

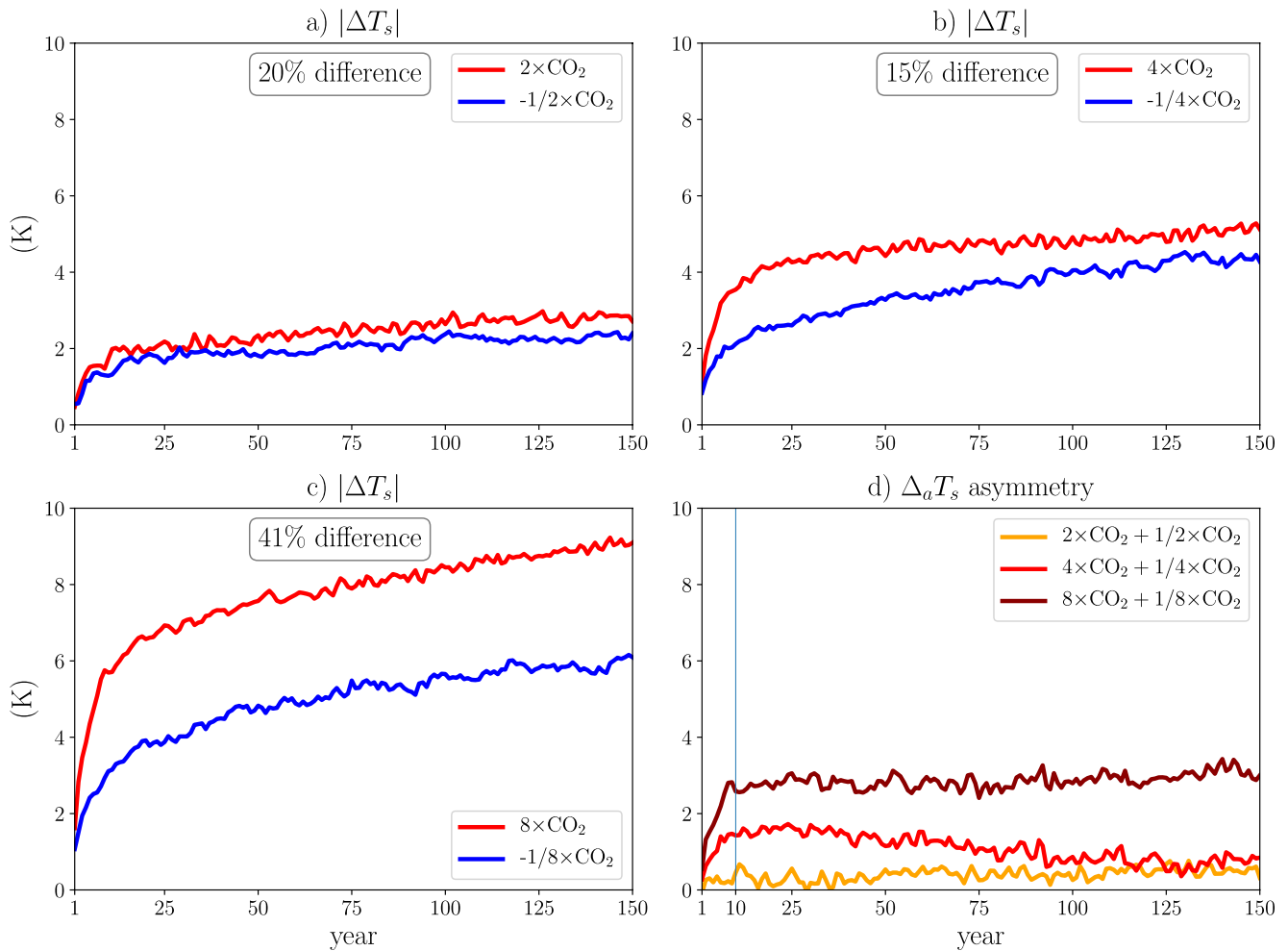


**Figure 1.** Timeseries of surface temperature response ( $|\Delta T_s|$ ) for abrupt  $\text{CO}_2$  runs with Community Earth System Model (CESM-LE). (a)  $2\times\text{CO}_2$  and  $1/2\times\text{CO}_2$ , (b)  $4\times\text{CO}_2$  and  $1/4\times\text{CO}_2$ , (c)  $8\times\text{CO}_2$  and  $1/8\times\text{CO}_2$  runs, and (d) surface temperature asymmetry ( $\Delta_a T_s$ ) between “warm” and “cold” cases.

note that the  $|\Delta T_s|$  in the “warm” case is always stronger than the “cold” case. In particular, we find 20% more warming at  $2\times$  than cooling at  $1/2\times\text{CO}_2$  (Figure 1a), 15% more at  $4\times$  than  $1/4\times\text{CO}_2$  (Figure 1b), and 41% more at  $8\times$  than  $1/8\times\text{CO}_2$  (Figure 1c). The asymmetry in  $|\Delta T_s|$  is amplified at higher  $\text{CO}_2$  forcing, and largest in the  $1/8\times\text{CO}_2$  versus  $8\times\text{CO}_2$  case (Figure 1c). The asymmetry is reduced at  $4\times\text{CO}_2$  versus  $1/4\times\text{CO}_2$  due to changes in ocean heat transport which result in a formation of the North Atlantic Warming Hole in this model at  $4\times\text{CO}_2$  (see more details in Mitevski et al. (2021)).

To quantify the timescale of the asymmetry in  $|\Delta T_s|$  between “warm” and “cold” cases, we define the asymmetry between “warm” and “cold” cases as

$$\Delta_a X = |\Delta X(\text{warm})| - |\Delta X(\text{cold})| \quad (3)$$

where  $X$  is any climate variable (e.g.,  $T_s$ ), and subscript  $a$  refers to “asymmetry” (Figure 1d). In particular, we find that the asymmetry emerges rapidly in the first 10 years (e.g., 90% at  $8\times\text{CO}_2$ ). Relative to the (slower) response associated with SST-driven feedbacks, the asymmetry appears quickly, suggesting that it might be due to radiative changes.

Next, we calculate effective climate sensitivity  $S_G$  from the Gregory regression (Equation 1), and plot it as percentage change from  $2\times\text{CO}_2$  (black line, Figure 2a).  $S_G$  is  $\text{CO}_2$  dependent and increases with  $\text{CO}_2$  concentration: at  $1/8\times\text{CO}_2$ , it is more than 20% lower than  $2\times\text{CO}_2$  values, and at  $8\times\text{CO}_2$ , it is around 5% higher than at

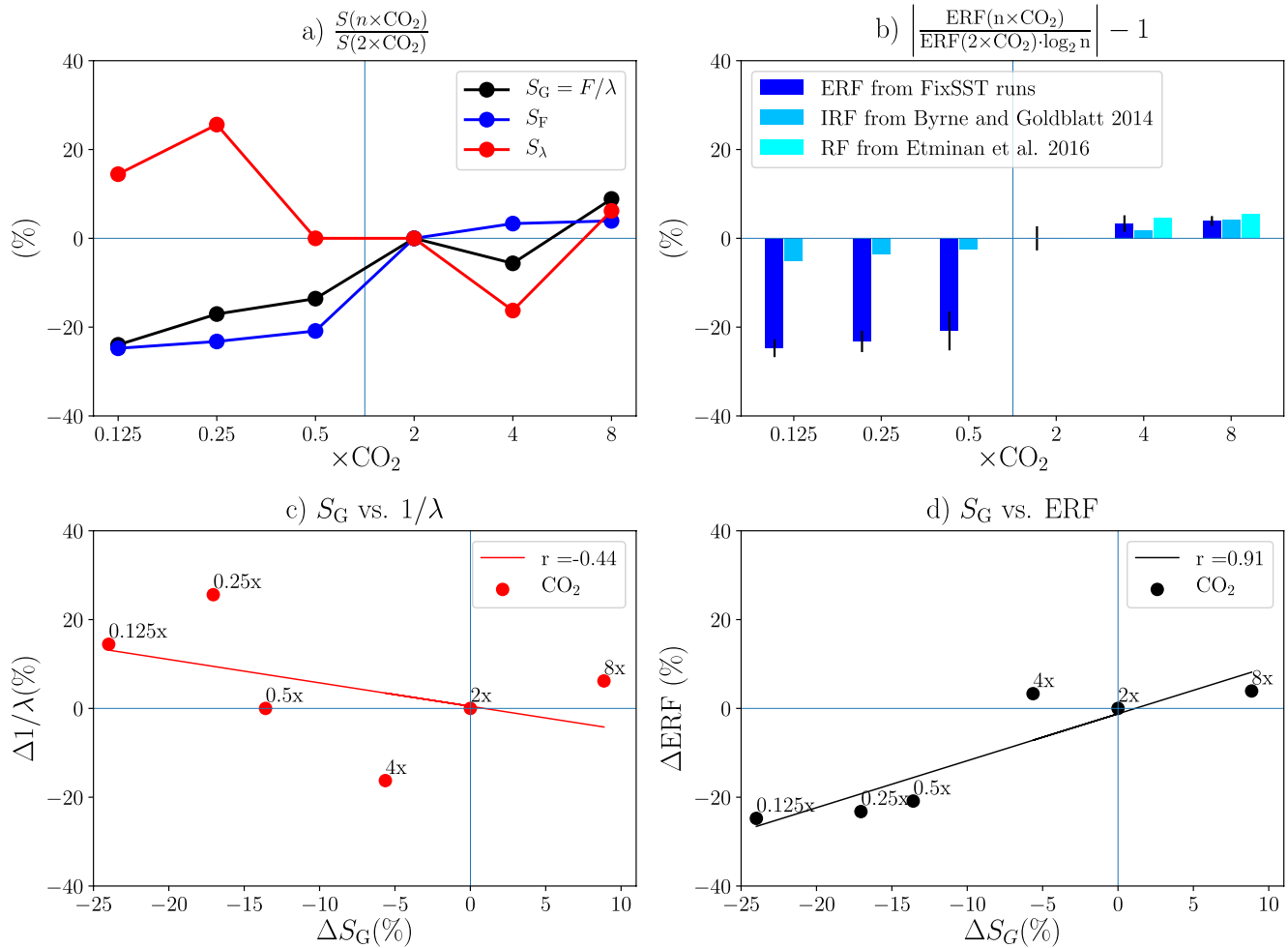


**Figure 2.** Percent change (from  $2\times CO_2$ ) for abrupt  $CO_2$  runs with CESM-LE of: (a) climate sensitivity as  $x$ -intercept of Gregory Regression (black,  $S_G$ ), as a function of ERF (blue,  $S_F$ ), and as a function of  $1/\lambda$  (red,  $S_\lambda$ ); (b) effective radiative forcing (dark blue, ERF), instantaneous radiative forcing (IRF) fit from Byrne and Goldblatt (2014) (light blue), and stratospherically adjusted radiative forcing (RF) fit from Etminan et al. (2016) (cyan). (c) Percent change of  $S_G$  versus  $1/\lambda$  (red) and (d)  $S_G$  versus effective radiative forcing (black).  $r$  is the Pearson correlation coefficient.

$2\times CO_2$ .  $CO_2$  dependent  $S_G$  is possible if either the ERF or the net feedback parameter ( $\lambda$ ) change with  $CO_2$ . To individually test the relative importance of ERF and  $\lambda$ , we calculate the climate sensitivity in two different ways.

First, to examine the dependence of climate sensitivity on ERF, we calculate climate sensitivity as  $S_F$  using the expression:

$$S_F = \left| \frac{ERF(n \times CO_2)}{\lambda(2 \times CO_2) \cdot \log_2 n} \right| \quad (4)$$

where ERF is derived from the  $n \times CO_2$  fixed SSTs and SICs runs, and  $\lambda$  (slope from Gregory Regression) is held constant at the  $2\times CO_2$  value. As seen in Figure 2a, we find that  $S_F$  (blue line) changes in tandem with  $S_G$  (black line), which reinforces the fact that changes in ERF explain the changes in  $S_G$ .

Second, to assess whether changes in feedback strength also contribute to  $S_G$ , we calculate climate sensitivity as  $S_\lambda$ :

$$S_\lambda = \left| \frac{ERF(2 \times CO_2)}{\lambda(n \times CO_2)} \right| \quad (5)$$

where  $\lambda$  is calculated at each  $n \times \text{CO}_2$  and ERF is held constant at  $2 \times \text{CO}_2$  value. As seen in Figure 2a,  $S_\lambda$  (red) changes in the opposite direction than  $S_G$  (black) for  $\text{CO}_2$  values lower than  $2 \times \text{CO}_2$ . This suggests that changes in  $\lambda$  are not the main driver of the  $S_G$  dependence on  $\text{CO}_2$ . However, it is important to note that for  $\text{CO}_2$  values higher than  $2 \times \text{CO}_2$ , we find  $\lambda$  non-monotonically increasing to  $8 \times \text{CO}_2$ , which can be linked to the corresponding non-monotonic behavior of  $S_G$ . We find qualitatively similar results using the GISS-E2.1-G model (Figure S2a in Supporting Information S1), confirming that ERF is the primary driver of the dependence of  $S_G$  on  $\text{CO}_2$ .

Next, we correlate  $S_G$  with  $1/\lambda$  (Figure 2c) and ERF (Figure 2d) across all abrupt  $\text{CO}_2$  experiments from  $1/8 \times$  to  $8 \times \text{CO}_2$  to examine whether feedbacks or forcing better correlate with changes in  $S_G$ . Overall, we find little correlation between  $S_G$  and  $1/\lambda$  ( $r = -0.44$ ) and a very strong correlation between  $S_G$  and ERF ( $r = 0.91$ ). Similarly, a high correlation between  $S_G$  and ERF is found in the GISS-E2.1-G model (Figure S2d in Supporting Information S1). This strengthens our conclusions from Figure 2a that the changes in ERF are driving the  $S_G$  increase. However, if one considers warm cases, one sees a strong correlation between  $S_G$  and  $1/\lambda$ , as indicated earlier. This is in agreement with previous studies (Bloch-Johnson et al., 2021; Meraner et al., 2013), which reported that feedback changes are important for the dependence of  $S_G$  on  $\text{CO}_2$ . However, over a broad range of  $\text{CO}_2$  forcing, including colder climates, that is not the case: changes in ERF are more important than feedback changes.

Given the aforementioned importance of ERF in driving the changes in  $S_G$ , we next look in more detail at ERF, calculated from fixed SSTs and SICs runs, following Forster et al. (2016), from  $1/8 \times$  to  $8 \times \text{CO}_2$  (dark blue bars, Figure 2b). If ERF were scaled simply with the logarithm of  $\text{CO}_2$  concentration, then the dark blue bars would be identical for all  $\text{CO}_2$  values. However, we see that ERF grows more than logarithmically with  $\text{CO}_2$ . We find a similar but weaker non-logarithmic behavior in the instantaneous radiative forcing (IRF) reported in Byrne and Goldblatt (2014), which we obtain by linearly interpolating their line-by-line radiative calculations (SI file “text03.txt” in Byrne and Goldblatt (2014)) and plot with light blue bars in Figure 2b. We also compare our ERF calculations with the proposed stratospherically adjusted radiative forcing fit in Etminan et al. (2016) for the warming case only (since it is not valid for low  $\text{CO}_2$  values), and it appears both are in agreement.

A limitation to our ERF calculation approach is that we only fix the SSTs and SICs in the simulation, but not the land temperatures. Fixing the land temperatures has been shown to increase ERF in warmer climates even more than when only SSTs and SICs are fixed (Andrews et al., 2021). To account for this, we removed the land and sea-ice warming effects in our ERF calculations, following Equation 1 in Hansen et al. (2005) as shown in Figure S3 in Supporting Information S1, and found that the correction (dashed blue lines) leads, if anything, to a stronger non-logarithmic ERF. Hence, incorporating fixed land temperatures leads to ERF increasing even more rapidly than the log of  $\text{CO}_2$  concentration; this strengthens our argument that the  $S_G$  dependence on  $\text{CO}_2$  is due to non-logarithmic  $\text{CO}_2$  radiative forcing.

Next, we perform a standard decomposition of  $\lambda$  into individual radiative feedbacks  $\lambda_i$ . The summation of individual feedbacks ( $\sum \lambda_i$ ) is shown in Figure 3a (blue).  $\sum \lambda_i$  follows closely the net feedback calculated from the Gregory regression (black). We perform the decomposition using two radiative kernels from Huang et al. (2017) and Pendergrass et al. (2018), and we find minimal sensitivity to the choice of kernel (Figure S4 in Supporting Information S1). The individual feedbacks, plotted as differences from  $2 \times \text{CO}_2$  values, from the Pendergrass et al. (2018) kernels are shown in Figure 3b. We see a clear signal in the lapse rate feedback, which weakens the net feedback in the “cold” case and strengthens it in the “warm” case. The longwave cloud feedback has clear global surface temperature dependence, increasing with  $\text{CO}_2$  monotonically for all  $\text{CO}_2$  values. However, in general, we find no clear pattern in the changes in individual feedbacks that would sufficiently explain the overall feedbacks  $\text{CO}_2$  dependence. In addition, the changes in feedbacks in the GISS-E2.1-G model (Figure S5 in Supporting Information S1) are qualitatively different from those in the CESM-LE model (Figure 3). Since our models do not agree on the changes in individual feedbacks across the  $\text{CO}_2$  range, and since we showed that feedback changes are strongly not correlated with changes in  $S_G$  (Figure 2c), we do not explore further the mechanisms driving feedback changes in the individual models.

### 3.2. Transient $\text{CO}_2$ Runs

The abrupt  $\text{CO}_2$  forcing runs show that the effective climate sensitivity increases with  $\text{CO}_2$ , and that the non-logarithmic nature of the ERF is largely responsible for this behavior. Now we seek to determine whether the same behavior is also seen in runs with transient  $\text{CO}_2$  forcing, which are much more realistic. Our transient runs are



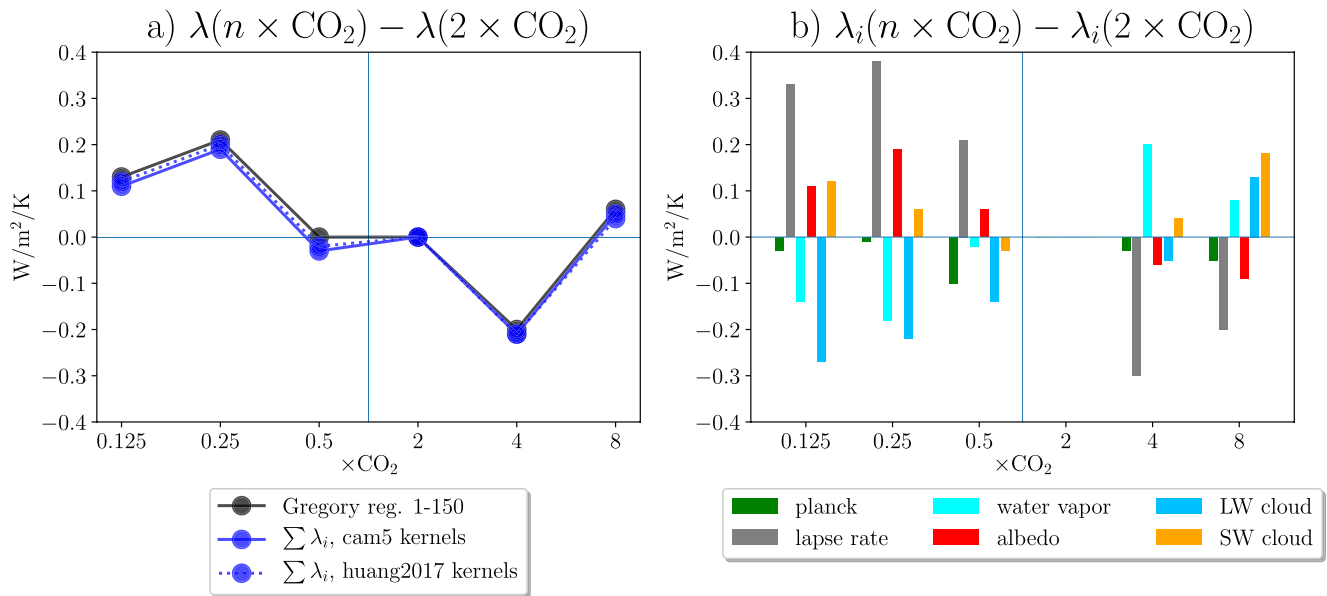


**Figure 3.** Feedbacks for abrupt CO<sub>2</sub> runs with CESM-LE are shown as a difference from 2×CO<sub>2</sub>. (a) Total feedback calculated with Gregory Regression years 1–150 (black), Pendergrass et al. (2018) kernels for CESM1-CAM5 (blue solid), and Huang et al. (2017) kernels (blue dashed). (b) Individual feedbacks calculated with Pendergrass et al. (2018) kernels.

forced, starting from PI, with CO<sub>2</sub> concentrations increasing at the rate of 1%yr<sup>-1</sup> and decreasing at 1%yr<sup>-1</sup>. As seen in Figure 4a, the surface temperature response  $|\Delta T_s|$  is stronger in the warming (red) than in the cooling (blue) case. Note that the responses computed from the last 50 years of the abrupt simulations at the corresponding CO<sub>2</sub> value (dots) are a good predictor of the response in the transient runs, demonstrating that the results of the abrupt runs carry over to the transient runs. Together with the surface temperature, ERF also changes more rapidly in the warming than the cooling experiments, as seen in Figure 4b.

Next, we explore how the transient feedbacks ( $\lambda_{tr}$ , see Equation 2) change in the “warm” and “cold” cases (Figure 4c). The feedbacks timeseries are noisy at the beginning of the simulation, but in the last 30 years, the warm case shows 10% weaker (more positive) feedbacks compared to the cold case. The 10% difference indicates that  $S_G$  in the warming case should be higher than in the colder case. However, a robust difference in feedbacks only appears around year 130, whereas the  $|\Delta T_s|$  asymmetry emerges much earlier, around year 60. This difference in the temporal evolution of the feedbacks, relative to the evolution of the forcing and  $S_G$ , adds additional strong evidence that the feedbacks are not driving the  $|\Delta T_s|$  asymmetry.

Finally, as for the abrupt CO<sub>2</sub> runs, we correlate the asymmetry in global mean surface temperature response  $\Delta_a T_s$  and effective radiative forcing  $\Delta_a \text{ERF}$  (Figure 4d). We find a correlation of  $r = 0.96$ , suggesting that the asymmetric changes in ERF drive the  $|\Delta T_s|$  asymmetry between the “cold” and “warm” cases. As we can see in Figure 4c, the transient feedbacks are contributing to the  $|\Delta T_s|$  asymmetry at the end of the run, but their impact is much smaller than the one from ERF.

#### 4. Summary and Discussion

We have explored the effective climate sensitivity ( $S_G$ ) dependence on CO<sub>2</sub> with abrupt *and* transient CO<sub>2</sub> experiments spanning the range 1/8× to 8×CO<sub>2</sub> using two distinct CMIP-class climate models. First, we have found a considerable asymmetry in surface temperature response, with the climate system warming more than cooling for identical factors used to increase and decrease the CO<sub>2</sub> concentration, starting from a PI climate. Second, we showed that the asymmetry is due to the non-logarithmic nature of CO<sub>2</sub> radiative forcing, not the feedback changes. Upon decomposing the total feedback into individual feedbacks, we found no simple explanation relating specific feedback changes to the changes in  $S_G$  across the 1/8× to 8× CO<sub>2</sub> forcing range examined in this study.

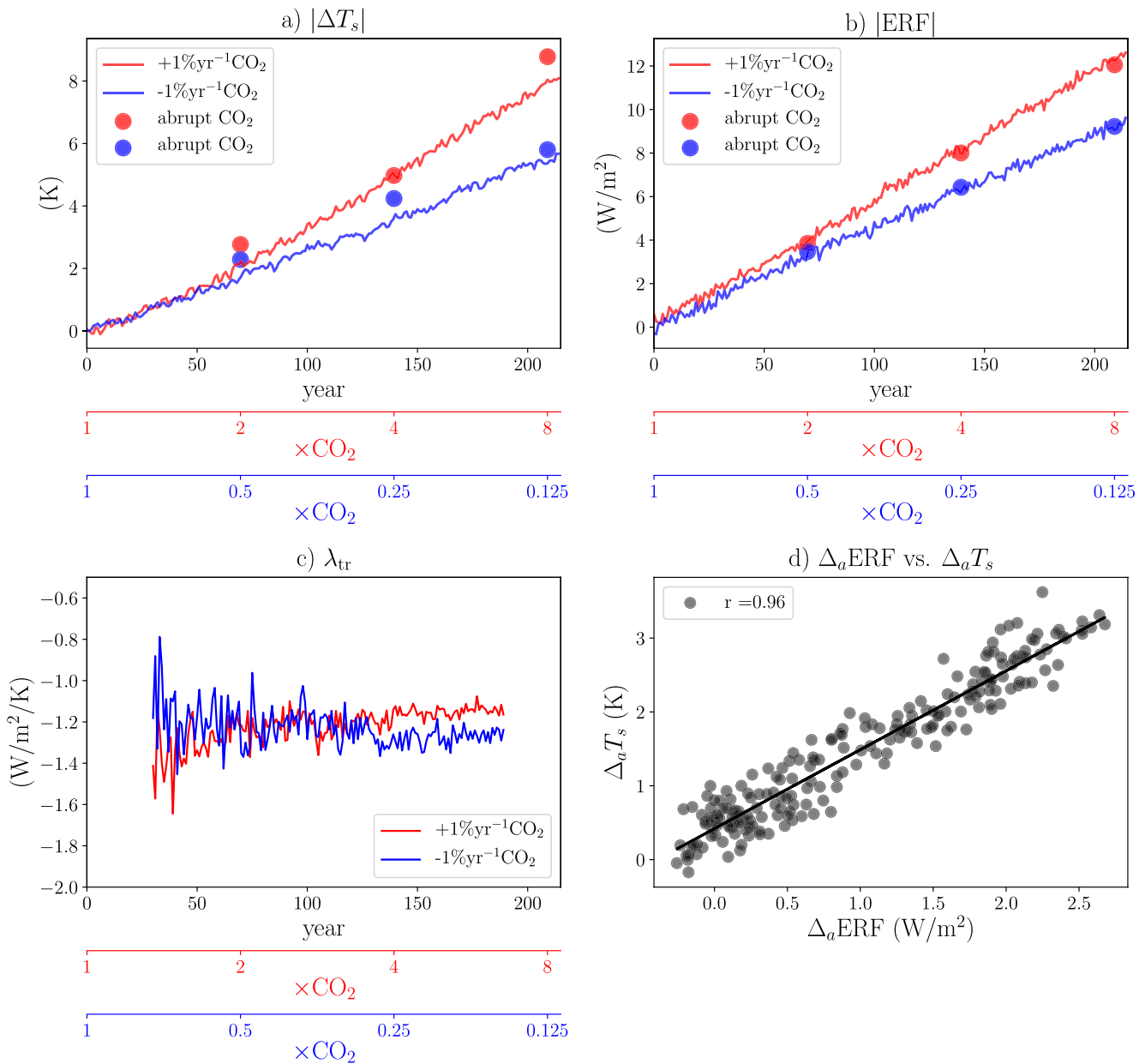


**Figure 4.** Transient runs annual timeseries with CESM-LE of (a) the absolute value of surface temperature response ( $|\Delta T_s|$ ), (b) effective radiative forcing ( $|ERF|$ ), (c) net feedback ( $\lambda_{tr}$ ), and (d) correlation between asymmetries in  $\Delta_a T_s$  and  $\Delta_a ERF$ . Responses from abrupt simulations are shown as dots.

Most studies to date have focused on the role of feedbacks in explaining the dependency of  $S_G$  on  $CO_2$ , with relatively little attention placed on radiative forcing. Indeed, consistent with these studies, we found that for warmer climates ( $>2 \times CO_2$ ), feedbacks are important for determining the changing behavior of  $S_G$  with  $CO_2$ . However, by considering a broader range of  $CO_2$  forcings, we have shown here that for cases in which  $CO_2$  concentrations are less than PI values, non-logarithmic ERF is the primary driver of  $S_G$  changes. Our goal here has been to isolate the role of  $CO_2$  alone, and we have set all other forcings to PI values. Needless to say, we have ignored the “slow” feedbacks present in cold climates (e.g., the LGM), such as the formation of land ice sheets.

The results with our abrupt runs have been shown to be robust with two climate models for simulations up to 150 years. One may argue that our runs are not equilibrated, and we agree with that caveat. However, we have found that the asymmetry and the key role of ERF are also robustly seen in the transient runs. Because of this, we expect that prolonging the abrupt simulation for more than 150 years will yield similar results. In any case, it will



be important to repeat similar experiments with longer simulations as in LongRunMIP (Rugenstein et al., 2019) to confirm that this asymmetry is still present at long times closer to equilibration. Finally, our findings indicate that future studies should place more emphasis on accurately quantifying the changes in ERF when studying the effective climate sensitivity dependency on CO<sub>2</sub>. The feedbacks appear unable to explain the cooling phase.

## Data Availability Statement

Part of the computing and data storage resources, including the Cheyenne supercomputer (<https://doi.org/10.5065/D6RX99HX>), were provided by the Computational and Information Systems Laboratory at National Center for Atmospheric Research (NCAR). The CESM-LE model data can be obtained at <https://doi.org/10.5281/zenodo.5725084> and GISS-E2.1-G model data at <https://doi.org/10.5281/zenodo.3901624>.

## Acknowledgments

We thank Jennifer Kay (University of Colorado Boulder) for helping with the feedback calculations, Ian Eisenman (UC San Diego) and Kyle Armour (University of Washington) for suggesting the radiative forcing fit from Byrne and Goldblatt (2014), and two anonymous reviewers for constructive comments that improved the paper. This work was supported by NASA FINESST Grant 80NSSC20K1657. The work of LMP is supported, in part, by a grant from the US National Science Foundation to Columbia University. We thank the high-performance computing resources provided by NASA's Advanced Supercomputing (NAS) Division and the NASA Center for Climate Simulation (NCCS).

## References

- Anagnostou, E., John, E. H., Babila, T. L., Sexton, P. F., Ridgwell, A., Lunt, D. J., et al. (2020). Proxy evidence for state-dependence of climate sensitivity in the Eocene greenhouse. *Nature Communications*, 11(1), 4436. <https://doi.org/10.1038/s41467-020-17887-x>
- Anagnostou, E., John, E. H., Edgar, K. M., Foster, G. L., Ridgwell, A., Inglis, G. N., et al. (2016). Changing atmospheric CO<sub>2</sub> concentration was the primary driver of early Cenozoic climate. *Nature*, 533(7603), 380–384. <https://doi.org/10.1038/nature17423>
- Andrews, T., Smith, C. J., Myhre, G., Forster, P. M., Chadwick, R., & Ackerley, D. (2021). Effective radiative forcing in a gcm with fixed surface temperatures. *Journal of Geophysical Research: Atmospheres*, 126(4), e2020JD033880. <https://doi.org/10.1029/2020JD033880>
- Bloch-Johnson, J., Rugenstein, M., Stolpe, M. B., Rohrschneider, T., Zheng, Y., & Gregory, J. M. (2021). Climate sensitivity increases under higher co2 levels due to feedback temperature dependence. *Geophysical Research Letters*, 48(4), e2020GL089074. <https://doi.org/10.1029/2020GL089074>
- Byrne, B., & Goldblatt, C. (2014). Radiative forcing at high concentrations of well-mixed greenhouse gases. *Geophysical Research Letters*, 41(1), 152–160. <https://doi.org/10.1002/2013GL058456>
- Caballero, R., & Huber, M. (2013). State-dependent climate sensitivity in past warm climates and its implications for future climate projections. *Proceedings of the National Academy of Sciences*, 110(35), 14162–14167. <https://doi.org/10.1073/pnas.1303365110>
- Chalmers, J., Kay, J. E., Middlemas, E., Maroon, E., & DiNezio, P. (2022). Does disabling cloud radiative feedbacks change spatial patterns of surface greenhouse warming and cooling? *Journal of Climate*, 1–60. <https://doi.org/10.1175/JCLI-D-21-0391.1>
- Colman, R., & McAvaney, B. (2009). Climate feedbacks under a very broad range of forcing. *Geophysical Research Letters*, 36(1). <https://doi.org/10.1029/2008GL036268>
- Etminan, M., Myhre, G., Highwood, E. J., & Shine, K. P. (2016). Radiative forcing of carbon dioxide, methane, and nitrous oxide: A significant revision of the methane radiative forcing. *Geophysical Research Letters*, 43(24), 12614–12623. <https://doi.org/10.1002/2016GL071930>
- Farnsworth, A., Lunt, D. J., O'Brien, C. L., Foster, G. L., Inglis, G. N., Markwick, P., et al. (2019). Climate sensitivity on geological timescales controlled by nonlinear feedbacks and ocean circulation. *Geophysical Research Letters*, 46(16), 9880–9889. <https://doi.org/10.1029/2019GL083574>
- Forster, P., Richardson, T., Maycock, A. C., Smith, C. J., Samset, B. H., Myhre, G., et al. (2016). Recommendations for diagnosing effective radiative forcing from climate models for cmip6. *Journal of Geophysical Research: Atmospheres*, 121, 12460–12475. <https://doi.org/10.1002/2016JD025320>
- Friedrich, T., Timmermann, A., Tigchelaar, M., Elison Timm, O., & Ganopolski, A. (2016). Nonlinear climate sensitivity and its implications for future greenhouse warming. *Science Advances*, 2(11). <https://doi.org/10.1126/sciadv.1501923>
- Gregory, J. M., Ingram, W. J., Palmer, M. A., Jones, G. S., Stott, P. A., Thorpe, R. B., & Williams, K. D. (2004). A new method for diagnosing radiative forcing and climate sensitivity. *Geophysical Research Letters*, 31(3). <https://doi.org/10.1029/2003GL018747>
- Hansen, J., Sato, M., Ruedy, R., Nazarenko, L., Lacis, A., Schmidt, G. A., & Zhang, S. (2005). Efficacy of climate forcings. *Journal of Geophysical Research: Atmospheres*, 110(D18). <https://doi.org/10.1029/2005JD005776>
- Huang, Y., Xia, Y., & Tan, X. (2017). On the pattern of co2 radiative forcing and poleward energy transport. *Journal of Geophysical Research: Atmospheres*, 122, 10578–10593. <https://doi.org/10.1002/2017JD027221>
- Kay, J. E., Deser, C., Phillips, A., Mai, A., Hannay, C., Strand, G., et al. (2015). The community earth system model (CESM) large ensemble project: A community resource for studying climate change in the presence of internal climate variability. *Bulletin of the American Meteorological Society*, 96(8), 1333–1349. <https://doi.org/10.1175/BAMS-D-13-00255.1>
- Kelley, M., Schmidt, G. A., Nazarenko, L. S., Bauer, S. E., Ruedy, R., Russell, G. L., et al. (2020). Giss-e2.1: Configurations and climatology. *Journal of Advances in Modeling Earth Systems*, 12(8), e2019MS002025. <https://doi.org/10.1029/2019MS002025>
- Martínez-Botí, M. A., Foster, G. L., Chalk, T. B., Rohling, E. J., Sexton, P. F., Lunt, D. J., et al. (2015). Plio-pleistocene climate sensitivity evaluated using high-resolution CO<sub>2</sub> records. *Nature*, 518(7537), 49–54. <https://doi.org/10.1038/nature14145>
- Mauritsen, T., Bader, J., Becker, T., Behrens, J., Bittner, M., Brokopf, R., et al. (2019). Developments in the mpi-m earth system model version 1.2 (mpi-esml.2) and its response to increasing CO<sub>2</sub>. *Journal of Advances in Modeling Earth Systems*, 11(4), 998–1038. <https://doi.org/10.1029/2018MS001400>
- Meraner, K., Mauritsen, T., & Voigt, A. (2013). Robust increase in equilibrium climate sensitivity under global warming. *Geophysical Research Letters*, 40(22), 5944–5948. <https://doi.org/10.1002/2013GL058118>
- Mitevski, I., Orbe, C., Chemke, R., Nazarenko, L., & Polvani, L. M. (2021). Non-monotonic response of the climate system to abrupt CO<sub>2</sub> forcing. *Geophysical Research Letters*, 48(6), e2020GL090861. <https://doi.org/10.1029/2020GL090861>
- Pendergrass, A. G., Conley, A., & Vitt, F. M. (2018). Surface and top-of-atmosphere radiative feedback kernels for CESM-CAM5. *Earth System Science Data*, 10(1), 317–324. <https://doi.org/10.5194/essd-10-317-2018>
- Rugenstein, M., & Armour, K. C. (2021). Three flavors of radiative feedbacks and their implications for estimating equilibrium climate sensitivity. *Geophysical Research Letters*, 48(15), e2021GL092983. <https://doi.org/10.1029/2021GL092983>

- Rugenstein, M., Bloch-Johnson, J., Abe-Ouchi, A., Andrews, T., Beyerle, U., Cao, L., et al. (2019). Longrunmip: Motivation and design for a large collection of millennial-length AOGCM simulations. *Bulletin of the American Meteorological Society*, 100(12), 2551–2570. <https://doi.org/10.1175/BAMS-D-19-0068.1>
- Russell, G. L., Lacis, A. A., Rind, D. H., Colose, C., & Opstbaum, R. F. (2013). Fast atmosphere-ocean model runs with large changes in CO<sub>2</sub>. *Geophysical Research Letters*, 40(21), 5787–5792. <https://doi.org/10.1002/2013GL056755>
- Shaffer, G., Huber, M., Rondanelli, R., & Pepke Pedersen, J. O. (2016). Deep time evidence for climate sensitivity increase with warming. *Geophysical Research Letters*, 43(12), 6538–6545. <https://doi.org/10.1002/2016GL069243>
- Shell, K. M., Kiehl, J. T., & Shields, C. A. (2008). Using the radiative kernel technique to calculate climate feedbacks in NCAR'S community atmospheric model. *Journal of Climate*, 21(10), 2269–2282. <https://doi.org/10.1175/2007JCLI2044.1>
- Sherwood, S. C., Webb, M. J., Annan, J. D., Armour, K. C., Forster, P. M., Hargreaves, J. C., et al. (2020). An assessment of earth's climate sensitivity using multiple lines of evidence. *Reviews of Geophysics*, 58. <https://doi.org/10.1029/2019RG000678>
- Smith, C. J., Kramer, R. J., Myhre, G., Alterskjær, K., Collins, W., Sima, A., et al. (2020). Effective radiative forcing and adjustments in CMIP6 models. *Atmospheric Chemistry and Physics*, 20(16), 9591–9618. <https://doi.org/10.5194/acp-20-9591-2020>
- Soden, B. J., & Held, I. M. (2006). An assessment of climate feedbacks in coupled ocean-atmosphere models. *Journal of Climate*, 19(14), 3354–3360. <https://doi.org/10.1175/JCLI3799.1>
- Soden, B. J., Held, I. M., Colman, R., Shell, K. M., Kiehl, J. T., & Shields, C. A. (2008). Quantifying climate feedbacks using radiative kernels. *Journal of Climate*, 21(14), 3504–3520. <https://doi.org/10.1175/2007JCLI2110.1>
- Tierney, J. E., Zhu, J., King, J., Malevich, S. B., Hakim, G. J., & Poulsen, C. J. (2020). Glacial cooling and climate sensitivity revisited. *Nature*, 584(7822), 569–573. <https://doi.org/10.1038/s41586-020-2617-x>
- Zhu, J., & Poulsen, C. J. (2021). Last glacial maximum (LGM) climate forcing and ocean dynamical feedback and their implications for estimating climate sensitivity. *Climate of the Past*, 17(1), 253–267. <https://doi.org/10.5194/cp-17-253-2021>
- Zhu, J., Poulsen, C. J., & Tierney, J. E. (2019). Simulation of EOCENE extreme warmth and high climate sensitivity through cloud feedbacks. *Science Advances*, 5(9). <https://doi.org/10.1126/sciadv.aax1874>